

REGULAR PAPER

Hydrogenated In–Ga–Zn–O thin-film transistors with anodized and fluorinated Al₂O₃ gate insulator for flexible devices

To cite this article: Syuya Kono *et al* 2021 *Jpn. J. Appl. Phys.* **60** SBBM05

View the [article online](#) for updates and enhancements.

You may also like

- [Low-Temperature Processed Metal-Semiconductor Field-Effect Transistor with In–Ga–Zn–O Channel Deposited by Ar+O₂+H₂ Sputtering](#)
Yusaku Magari and Mamoru Furuta
- [Highly moisture resistant Ga-doped ZnO films with textured surface for thin-film solar cells with indium codoping fabricated by ion plating with direct-current arc discharge](#)
Huaping Song, Junichi Nomoto, Hisao Makino *et al.*
- [Electrochemical Growth of ZnO Nanorod Arrays onto Transparent Conductive IZO:Ga Substrates](#)
Daniel Solís-Cortés, Francisco Martín, Ricardo Schrebler *et al.*



PRIME
PACIFIC RIM MEETING
ON ELECTROCHEMICAL
AND SOLID STATE SCIENCE

HONOLULU, HI
Oct 6–11, 2024

Abstract submission deadline:
April 12, 2024

Learn more and submit!

Joint Meeting of
The Electrochemical Society
•
The Electrochemical Society of Japan
•
Korea Electrochemical Society



Hydrogenated In–Ga–Zn–O thin-film transistors with anodized and fluorinated Al₂O₃ gate insulator for flexible devices

Syuya Kono¹, Yusaku Magari^{1,2} , Marin Mori¹, S. G. Mehadi Aman¹ , Norbert Fruehauf³, Hiroshi Furuta^{2,4} , and Mamoru Furuta^{1,2*}

¹Material Science and Engineering Course, Kochi University of Technology, Kami, Kochi 782-8502, Japan

²Center for Nanotechnology, Research Institute, Kochi University of Technology, Kami, Kochi 782-8502, Japan

³Institute for Large Area Microelectronics, University of Stuttgart, Stuttgart 70569, Germany

⁴Department of Electronic and Photonic Systems Engineering, Kochi University of Technology, Kami, Kochi 782-8502, Japan

*E-mail: furuta.mamoru@kochi-tech.ac.jp

Received October 12, 2020; revised December 26, 2020; accepted January 25, 2021; published online February 10, 2021

For the purpose of developing In–Ga–Zn–O (IGZO) thin-film transistors (TFTs) on a flexible substrate, low-temperature (150 °C) processed hydrogenated IGZO (IGZO:H) TFTs with anodized alumina gate insulator (Al₂O₃ GI) have been developed. We found that fluorination of the Al₂O₃ GI surface significantly improves field effect mobility (μ_{FE}) and positive gate bias and temperature stress (PBTS) reliability of the TFTs. μ_{FE} of 28.8 cm² V⁻¹ s⁻¹ and good PBTS reliability were obtained from the IGZO:H TFTs with a 68 nm thick fluorinated Al₂O₃ GI. X-ray photoelectron spectroscopy analysis revealed that fluorine in the AlOF_x formed at the Al₂O₃ surface played an important role in improving performance and PBTS reliability of low-temperature-processed oxide TFTs for future flexible device applications. © 2021 The Japan Society of Applied Physics

1. Introduction

Transparent metal oxide semiconductors have been extensively investigated as the active channel layers of thin-film transistors (TFTs) for next-generation flat-panel displays,^{1–3} nonvolatile memories,^{4,5} image sensors,^{6,7} pH sensors,^{8,9} metal-semiconductor field effect transistors,^{10–15} and so on. Especially, In–Ga–Zn–O (IGZO) is a promising candidate for the active channel of flexible TFTs since the IGZO exhibits an electron mobility of more than 10 cm² V⁻¹ s⁻¹ even when deposited at room temperature.^{16,17} However, IGZO TFTs generally require thermal annealing around 300 °C to reduce defects formed as a result of various types of processing damage.^{18–22} Our group reported that hydrogenated IGZO film, which is deposited by Ar + O₂ + H₂ sputtering, is very promising for the fabrication of oxide TFTs below the softening temperature of plastic substrates for future flexible device applications. Defects generated in as-deposited IGZO films can be reduced through the low-temperature (150 °C) annealing.^{15,23,24} The field-effect mobility (μ_{FE}) of 13.4²³ and 18.9²⁴ cm² V⁻¹ s⁻¹ were achieved for a IGZO:H TFTs with In:Ga:Zn ratios of 1:1:1 and 6:2:1 atm%, respectively, after 150 °C annealing. However, previous results of IGZO:H TFTs were used thermally grown SiO₂ as a gate insulator (GI).^{23,24} To apply IGZO:H TFTs on plastic substrates, a maximum processing temperature of GI should be reduced below the softening temperature of plastic substrates.

In this paper, an aluminum oxide (Al₂O₃) prepared by anodization^{25,26} is used as a GI for IGZO:H TFTs.^{27–29} Al₂O₃ has the advantages of high dielectric constant (~9) and low leakage current density, which are suitable for a GI in low-temperature processed IGZO TFTs. Moreover, anodization is conformal, pinhole free, self-limiting, and room temperature processes to make it compatible with flexible electronic devices. The fabricated IGZO621:H TFT with an anodized Al₂O₃ GI exhibited field effect mobility (μ_{FE}) of 28.1 cm² V⁻¹ s⁻¹, on/off current ratio of over 10⁷, and good positive bias temperature stress (PBTS) reliability. This is an extended version of the 2020 International Conference on Solid State Devices and Materials (SSDM2020) proceedings

paper.³⁰ In the present paper, we discuss the effects of post anodization treatment of Al₂O₃ GI on the performance and reliability of the TFTs in more detail.

2. Experimental methods

Figure 1 shows fabrication processing steps and a schematic cross-sectional view of the bottom-gate IGZO TFTs with an anodized Al₂O₃ GI. A 150 nm thick Al–Nd–Ti alloy was deposited by DC magnetron sputtering on 4 inch glass substrate, and was patterned into a gate electrode. An Al–Nd–Ti surface was anodized in an electrolyte (ammonium tartrate, ethylene glycol, and DI water) to form a 68 nm thick Al₂O₃ for GI. Anodization process was carried out under a constant current density (0.37 mA cm⁻²) at an applied voltage of 48 V. From X-ray photoelectron spectroscopy (XPS) analysis, an atomic ratio of O/Al in anodized Al₂O₃ film was 1.49, indicating a stoichiometric film. After the anodization, two types of post anodization treatments were applied to an Al₂O₃ GI. The first was a vacuum annealing at 150 °C for 1 h. The second was plasma fluorination of the Al₂O₃ surface. The plasma fluorination was carried out in an O₂ plasma used polytetrafluoroethylene (PTFE) as a fluorine source. An Al₂O₃ GI without treatment was used as a reference. Then, a 20 nm thick hydrogenated IGZO621 (denoted hereafter as IGZO621:H) was deposited by RF magnetron sputtering in an Ar + O₂ + H₂ ambient from an IGZO target with an In:Ga:Zn ratio of 6:2:1 mol%.²⁴ The O₂ and H₂ gas flow ratios, defined as R(O₂) = O₂/(Ar + O₂ + H₂) and R(H₂) = H₂/(Ar + O₂ + H₂), respectively, were set at 10% for R(O₂) and 9% for R(H₂) at a deposition pressure of 0.27 Pa. An IGZO621:H film was patterned into an active channel of the TFT by photolithography and wet etching. A permanent epoxy-based negative photoresist (SU-8)³¹ was spin-coated on the IGZO621:H as an organic passivation layer (OPVL) to exclude water and oxygen molecules in ambient air which degrade long-term and/or storage stability. After opening contact holes by an O₂ plasma etching, source and drain electrodes were formed by a stacked film of Mo/Al/Mo which was deposited by RF magnetron sputtering. Finally, the TFTs were subjected to annealing in air at 150 °C for 1 h. A maximum processing temperature of the

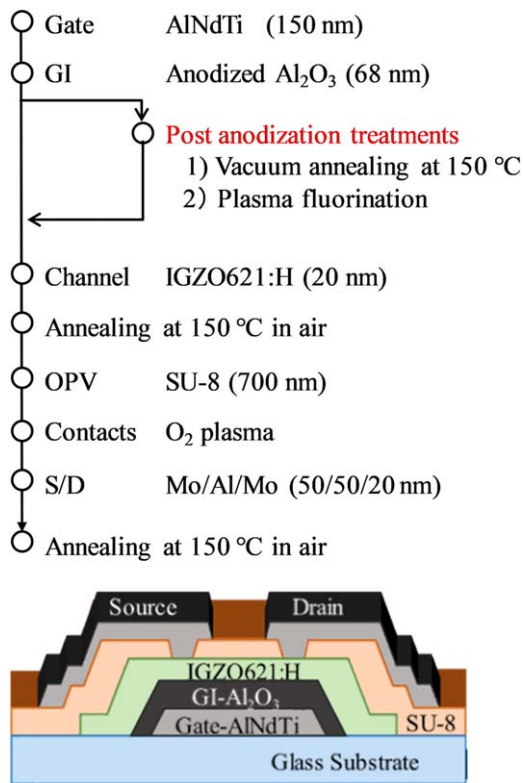


Fig. 1. (Color online) Fabrication processing steps and schematic cross-sectional view of the bottom-gate IGZO TFTs with an anodized Al₂O₃ GI.

TFTs was 150 °C. The channel length (L) and width (W) of the TFTs were 20 and 66 μm , respectively. The electrical properties and PBTS stability of the IGZO621:H TFTs with an Al₂O₃ GI were evaluated using a semiconductor parameter analyzer in darkness. Field effect mobility (μ_{FE}) of the TFT was extracted from the transconductance in a linear region at a drain voltage (V_{DS}) of 0.1 V. V_{th} was defined as the value of V_{GS} for a normalized drain current ($I_{\text{DS}} \times L/W$) of 1 nA to flow. The PBTS stability was measured at a stress temperature (T_{S}) of 60 °C with a gate voltage of +12 V up to a cumulative stress time of 6000 s.

3. Results and discussion

3.1. XPS surface analysis of anodized Al₂O₃ films without and with post anodization treatments

Figure 2 shows the XPS wide-scan spectra of the Al₂O₃ films without and with post anodization treatments. Al 2p, Al 2s, C 1s, and O 1s peaks were detected from the Al₂O₃ surface without post anodization treatment. After the vacuum annealing at 150 °C, no noticeable difference was found in the XPS spectra from the film without post anodization treatment. In contrast, the F 1s peak was clearly observed from the film after the plasma fluorination. Moreover, C 1s peak intensity was not increased so much after the plasma fluorination, suggesting no fluoropolymer deposition during the fluorination process.

3.2. Current density–electric field (J – E) characteristics of anodized Al₂O₃ films

Figure 3 shows the current density–electric field (J – E) characteristics of 68 nm thick anodized Al₂O₃ films with and without post anodization treatments. The J – E characteristics were measured by a metal–insulator–metal (Al/Al₂O₃/AlNdTi-ally) capacitor. Breakdown electric field (E_{BD}) was defined as the

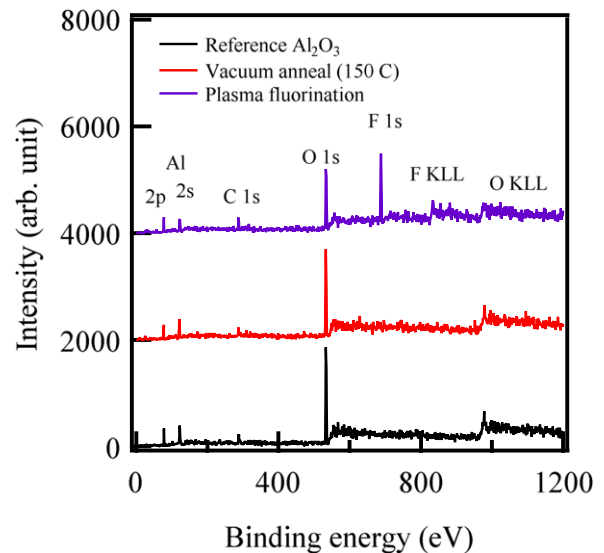


Fig. 2. (Color online) XPS wide-scan spectra of the Al₂O₃ films without, with vacuum annealing (150 °C), and with plasma fluorination.

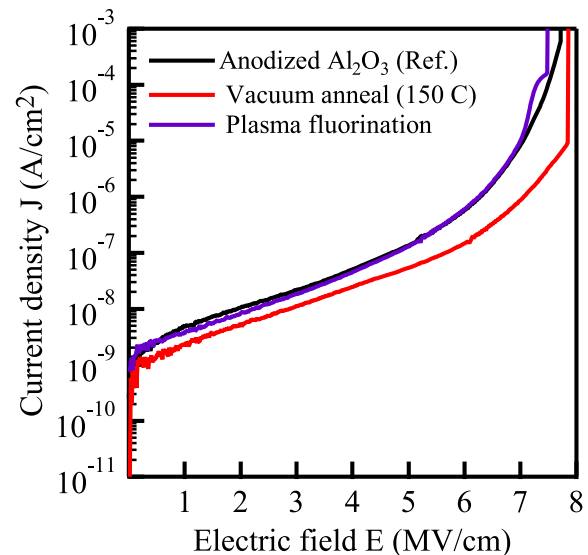


Fig. 3. (Color online) J – E characteristics of 68 nm thick anodized Al₂O₃ films without, with vacuum annealing (150 °C), and with plasma fluorination.

value of E for a current density of 1 $\mu\text{A cm}^{-2}$ to flow. The Al₂O₃ film with surface fluorination exhibited almost the same J – E characteristics with E_{BD} value of 6.3 MV cm⁻¹ as the reference film, indicating no influence of fluorine on J – E characteristics. On the other hand, current density slightly reduced, and E_{BD} improved to 7.1 MV cm⁻¹ when the film was annealed at 150 °C in vacuum. Dielectric constant, which was measured by a capacitance–voltage (C – V) measurement, were 9.0 for all films.

3.3. Electrical properties and PBTS reliability of IGZO621:H TFTs with anodized Al₂O₃ GI.

Figure 4 shows the transfer characteristics and the gate leakage current of the IGZO621:H TFTs with the Al₂O₃ GIs. Electrical properties of the TFTs are summarized in Table I. Reference TFT without post anodization treatment of the Al₂O₃ GI showed μ_{FE} value of 22.2 cm² V⁻¹ s⁻¹; however, large clockwise hysteresis (V_{H}) of 3.2 V was observed. The gate voltage (V_{GS}) dependence of μ_{FE} was also shown in Fig. 5(b). μ_{FE} of reference TFT first increased

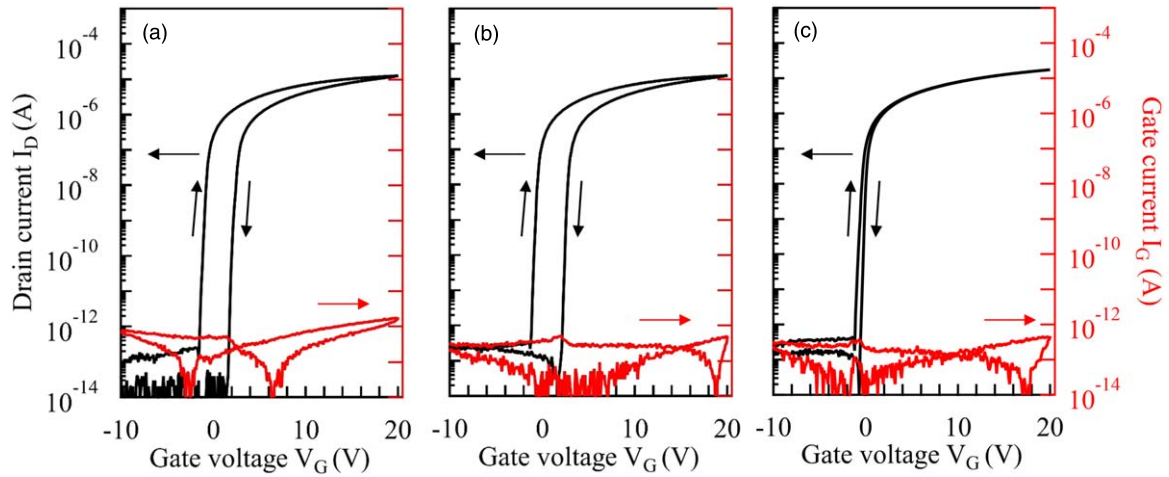


Fig. 4. (Color online) Transfer characteristics of IGZO621:H TFTs with the Al₂O₃ GIs (a) without post anodization process, (b) with vacuum annealing (150 °C), and (c) with plasma fluorination. Drain voltage is set at 0.1 V.

Table I. Summary of electrical properties and PBTS reliability of IGZO621:H TFTs with anodized Al₂O₃ GIs.

Post anodization treatment	μ_{FE} (cm ² V ⁻¹ s ⁻¹)	S.S. (V dec ⁻¹ .)	V _{th} (V)	V _H (V)	PBTS 6 ks ΔV_{th} (V)
None	22.2	0.14	-0.9	3.2	3.4
Vacuum anneal (150 °C)	22.5	0.15	-0.7	3.2	3.5
Plasma fluorination	28.1	0.17	-0.5	0.4	0.5

in the low- V_{GS} region, then it started to decrease as V_{GS} exceeded ~ 7 V. A maximum μ_{FE} value of 22.2 cm² V⁻¹ s⁻¹ was obtained at V_{GS} of ~ 7 V. For the TFT with the Al₂O₃ GI annealed at 150 °C in vacuum, both the μ_{FE} and the V_H values did not change from the reference TFT. The V_{GS} dependence of μ_{FE} in the TFT with the Al₂O₃ GI annealed at 150 °C in vacuum also followed a similar tendency as the reference TFT. In contrast, μ_{FE} value increased to 28.1 cm² V⁻¹ s⁻¹ and V_H value significantly improved to 0.4 V when the fluorinated Al₂O₃ film was used as a GI. μ_{FE} of the TFT with the fluorinated Al₂O₃ GI monotonically increased upon increasing V_{GS} of ~ 14 V, and a maximum μ_{FE} value of 28.1 cm² V⁻¹ s⁻¹ was obtained.

Figure 5 shows (a) V_H of the TFTs as a function of maximum V_{GS} upon applying transfer characteristics measurements and (b) V_{GS} dependence of the μ_{FE} of TFTs, respectively. For the reference TFT and the TFT with the Al₂O₃ GI annealed at 150 °C in vacuum, V_H values in both TFTs started to increase as V_{GS} exceeded ~ 8 V. The V_{GS}

values at which V_H started to increase are correlated well with the V_{GS} values at which μ_{FE} started to decrease. Since the hysteresis is originated from an electron trapping at an IGZO621:H/GI interface, Coulomb scattering of trapped electrons at the IGZO/Al₂O₃ interface would be a main cause for reducing μ_{FE} in high V_{GS} region for both the reference TFT and the TFT with the Al₂O₃ GI annealed at 150 °C in vacuum. In contrast, V_H values in the TFT with the fluorinated Al₂O₃ GI did not increase upon applying V_{GS} of 20 V. This result indicated that the electron trapping at the IGZO/Al₂O₃ interface or in the Al₂O₃ GI could be suppressed by the fluorination process. Thus, μ_{FE} of the TFT with the fluorinated Al₂O₃ GI increased with increasing V_{GS} , and maximum μ_{FE} value of 28.1 cm² V⁻¹ s⁻¹ was obtained at high V_{GS} of ~ 14 V. Thanks to a high gate capacitance of the Al₂O₃ GI, obtained μ_{FE} value is much larger than our previous report (18.9 cm² V⁻¹ s⁻¹) obtained from the IGZO621:H TFTs with a 100 nm thick thermally grown SiO₂ GI.²⁴⁾

Figure 6 shows the changes in transfer characteristics of the IGZO621:H TFTs with the Al₂O₃ GIs under PBTS tests. Both the reference TFT and the TFTs with the Al₂O₃ GI annealed at 150 °C in vacuum exhibited mostly the same degradation phenomena under PBTS test. After PBTS of 100 s, transfer curves shifted in a positive V_{GS} direction without degradation of a subthreshold swing. When a stress time further increased to 6000 s, transfer curves further shifted in the positive V_{GS} direction accompanied by the hump phenomenon. In contrast, PBTS reliability of the TFT markedly improved when the fluorinated Al₂O₃ film was used as a GI. After PBTS of 6000 s, transfer curve shifts, which was defined as the value of V_{GS} for a drain current of 10 μ A to flow, of the reference TFT and the TFT with the Al₂O₃ GI annealed at 150 °C in vacuum were 3.4 and 3.5 V, respectively, whereas that of the TFT with the fluorinated Al₂O₃ GI improved to 0.5 V. Furthermore, the hump

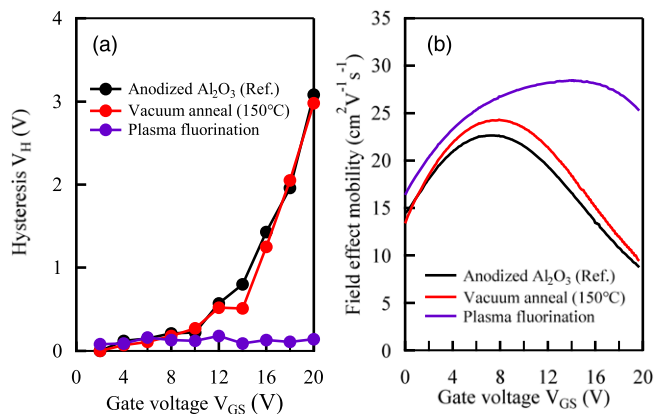


Fig. 5. (Color online) (a) Hysteresis and (b) μ_{FE} of IGZO621:H TFTs with the Al₂O₃ GIs without post anodization process, with vacuum annealing (150 °C), and with plasma fluorination as a function of applied gate voltage.

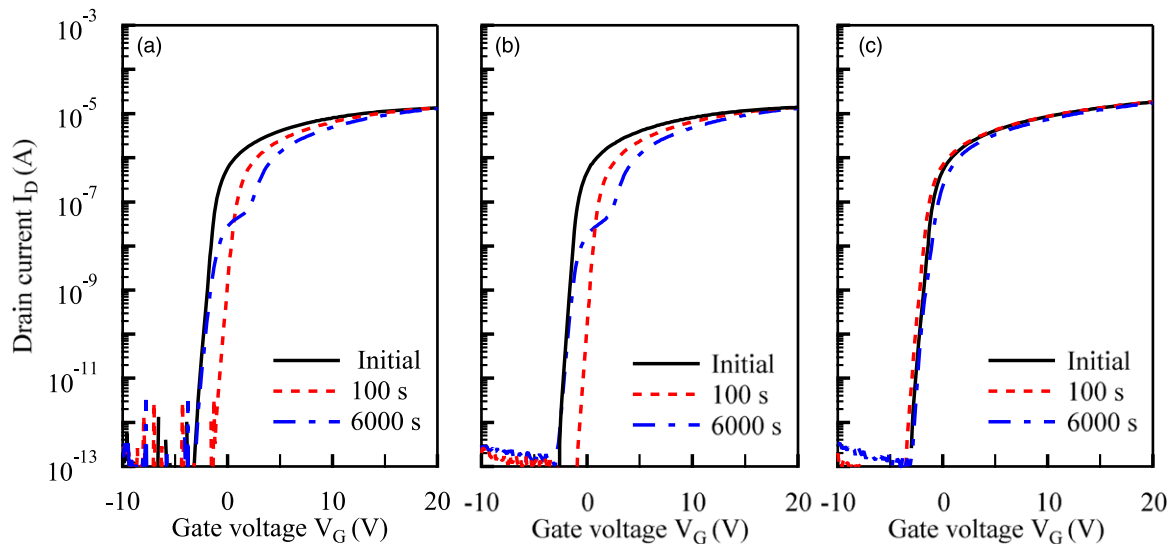


Fig. 6. (Color online) PBTS reliability of the IGZO621:H TFTs with the Al₂O₃ GI (a) without post-anodization process, (b) with vacuum annealing (150 °C), and (c) with plasma fluorination process. Gate voltage stress of 12 V was applied at 60 °C for 6 ks.

phenomenon was not observed after PBTS test for the TFT with the fluorinated Al₂O₃ GI.

It is worth noticing that although the Al₂O₃ films without and with the fluorination process exhibited almost the same *J*-*E* characteristics and *E*_{BD} values as shown in Fig. 3, μ_{FE} value and PBTS reliability of the TFT with the fluorinated Al₂O₃ GI markedly improved from the reference TFT. By using the fluorinated Al₂O₃ GI, μ_{FE} value of 28.1 cm² V⁻¹ s⁻¹ and excellent PBTS reliability were achieved for the IGZO621:H TFT fabricated at a maximum processing temperature of 150 °C.

3.4. Mechanism for improving electrical properties and PBTS reliability for IGZO621:H TFT with fluorinated Al₂O₃ GI

To understand the effects of the fluorination process of an anodized Al₂O₃ film on performance and reliability of the TFTs, surface roughness and chemical bonding states of the Al₂O₃ GI were analyzed by atomic force microscopy (AFM) and XPS, respectively.

Figure 7 shows AFM images of the Al₂O₃ films (a) without, (b) with vacuum annealing (150 °C), and (c) with plasma fluorination. All the films showed extremely smooth surface with root mean square roughness (*Rq*) values in the

range of 0.41–0.49 nm. This result indicates that the plasma fluorination has no influence on surface roughness of the Al₂O₃ film. In addition, no polymer deposition occurred during the plasma fluorination process.

Next, the chemical bonding states at the Al₂O₃ GI surface were investigated by XPS in detail. All the spectra were taken from the Al₂O₃ surface without an ion etching. Figure 8 shows the narrow-scan (a)–(c) Al 2p and (d)–(f) O 1s core spectra taken from the Al₂O₃ films without and with post-anodization treatments. The Al 2p spectra were well fitted by two Gaussian–Lorentz curves attributed to the Al–oxygen bonds (Al–O) at 75.0 eV and Al–hydroxides (Al–OH) at 75.9 eV, whereas the O 1s spectra were fitted by the metal–oxygen bonds (M–O) at 530.9 eV and oxygen in the hydroxides (–OH) at 532.5 eV.^{32–35} The full-width at half maximum of the Al–O and M–O peaks were set at 1.61 and 2.11 eV, respectively, while those of the Al–OH and –OH peaks were varied to reproduce the Al 2p and O 1s spectra. The absence of Al–Al bonds at 73 eV indicates a complete oxidation of all the Al₂O₃ surface by anodization. Table II summarizes the area ratios of M–O and –OH components in the Al 2p and O 1s peaks for the Al₂O₃ films with and without post-anodization treatments. For the Al₂O₃ film

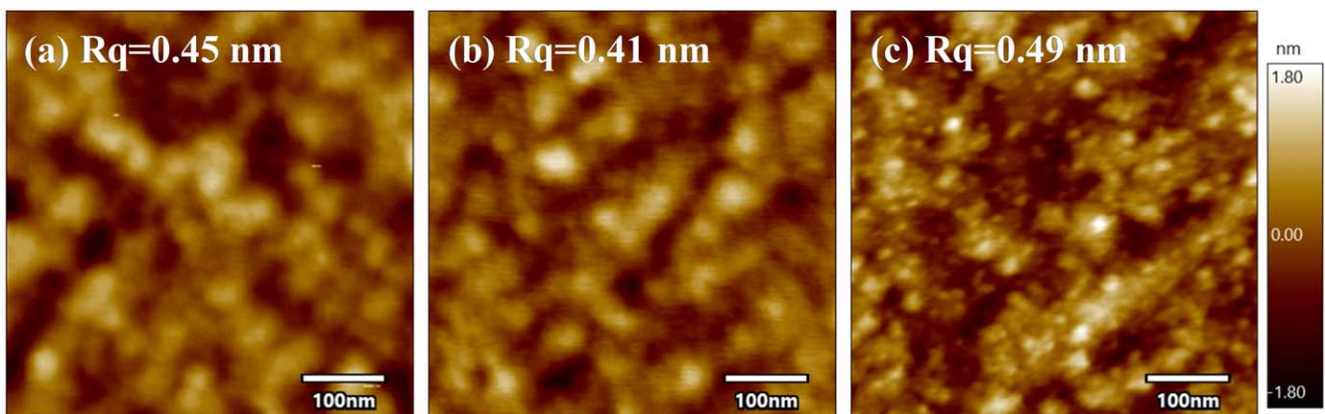


Fig. 7. (Color online) AFM images of the Al₂O₃ films (a) without post-anodization process, (b) with vacuum annealing (150 °C), and (c) with plasma fluorination.

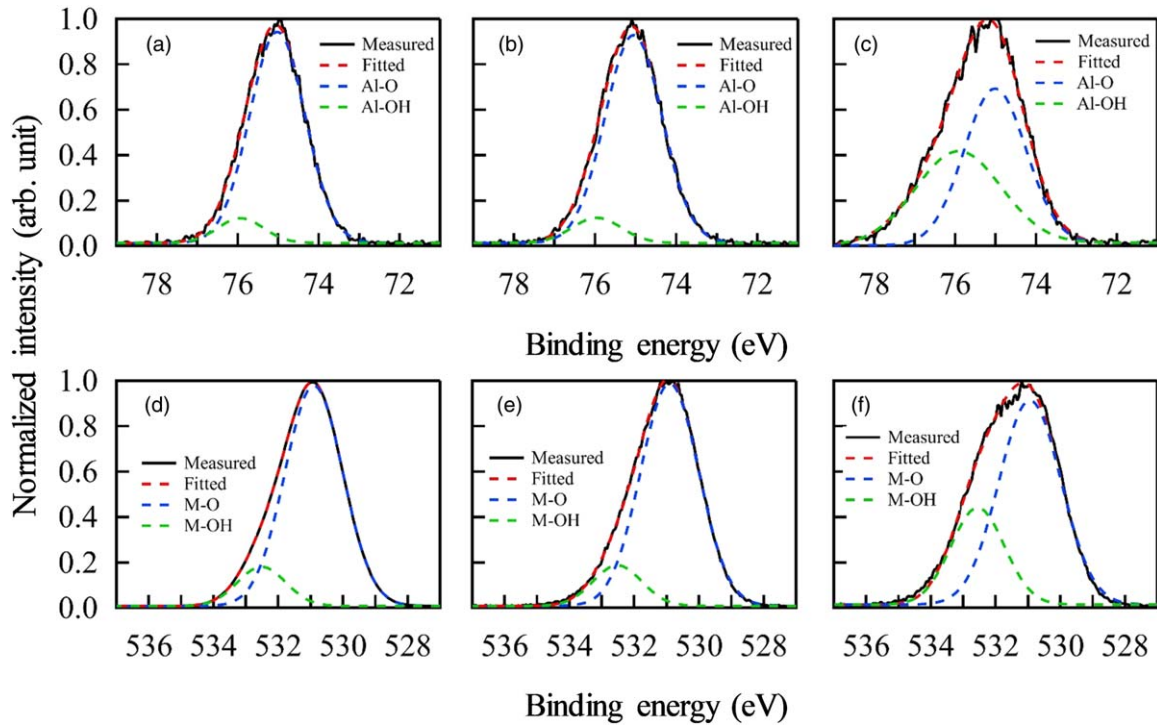


Fig. 8. (Color online) Narrow-scan spectra of (a)–(c) Al 2p and (d)–(f) O 1s in anodized Al₂O₃ films (a) (d) without, (b), (e) with vacuum annealing at 150 °C, and (c), (f) with plasma fluorination.

without post anodization process, area ratios of Al–OH in Al 2p and –OH in O 1s were 10.4% and 15.1%, respectively. The area ratios of Al–OH in Al 2p and –OH in O 1s did not change significantly after vacuum annealing of the Al₂O₃ film at 150 °C for 1 h; however, those components clearly increased after the plasma fluorination of anodized Al₂O₃ film. Higher energy component at 75.9 eV in Al 2p increased from 10.4% to 41.0%, while that at 532.5 eV in O 1s increased from 15.1% to 33.4% after the plasma fluorination. The increase of those higher energy components can not be assigned as the increase of OH components at the Al₂O₃ surface because the PTFE, which was used as fluorine source for plasma fluorination, does not contain hydrogen. The increase of those higher energy components in Al 2p and O 1s would be originated from Al and O atoms in fluorinated alumina (AlOF_x), respectively. The reported peak position of Al atoms in AlOF_x is 1.3 eV higher from the Al–O peak,³⁶⁾ at which is very close to Al–OH in Al 2p (75.9 eV). Based on the results obtained from Al 2p spectra, the increased higher energy component in O 1s spectrum after the plasma fluorination would also be originated from oxygen in fluorinated alumina (–OF_x). The AlF₃ component at 76.5 eV³⁶⁾ was not detected in Al 2p spectrum even after the plasma fluorination. We also

confirmed by XPS depth analysis that F was detected within 3 nm from the Al₂O₃ surface. Thus, it is reasonable to conclude that the fluorinated alumina was formed at the Al₂O₃ surface by the plasma fluorination. AFM and XPS results revealed that AlOF_x bonds were formed at an anodized Al₂O₃ surface without polymer deposition after the fluorination process. Since bond dissociation energy of Al–O is much higher than those of In–O, Ga–O, and Zn–O, oxygen vacancies would be formed at an IGZO/Al₂O₃ interface. Yamazaki et al. reported that fluorine introduced at an IGZO/fluorinated silicon nitride (SiN_x:F) GI interface lead to decrease of electron trap density and improve positive bias stress stability.³⁷⁾ Moreover, an introduction of fluorine in an IGZO suppressed not only the electron trapping at the IGZO/GI interface but also the creation of donor-like defects in an IGZO bulk.^{38–40)} Thus, fluorine in the AlOF_x formed at the Al₂O₃ surface played an important role in improving the performance and PBTS reliability of low-temperature-processed oxide TFTs for future flexible device applications.

4. Conclusions

Low-temperature processed IGZO621:H TFTs with an anodize Al₂O₃ GI have been demonstrated. *E*_{BD} value of

Table II. Summary of area ratios and FWHM of M–O and –OH components in the Al 2p and O 1s peaks for the Al₂O₃ films with and without post anodization treatments.

Post anodization treatment	Al 2p				O 1s			
	Al–O		Al–OH		M–O		–OH	
	Area ratio (%)	FWHM (eV)						
None	89.6	1.61	10.4	1.33	84.9	2.11	15.1	1.75
Vacuum anneal	88.1	1.61	11.9	1.33	84.5	2.11	15.5	1.76
Plasma fluorination	59.0	1.61	41.0	2.60	66.6	2.11	33.4	1.79

6.3 MV cm⁻¹ and dielectric constant of 9.0 were obtained from an anodized Al₂O₃ film. Fluorination of the anodized Al₂O₃ GI surface was carried out in an O₂ plasma used PTFE as a fluorine source. AFM and XPS results revealed that AlOF_x bonds were formed at an anodized Al₂O₃ GI surface without polymer deposition after the fluorination process. Fluorination of the Al₂O₃ GI surface reduces electron trapping sites at the IGZO621:H/Al₂O₃-GI interface or in the Al₂O₃ GI, result in improving both μ_{FE} and PBTS reliability of the TFTs. A μ_{FE} of 28.8 cm² V⁻¹ s⁻¹, a subthreshold swing of 0.17 V dec⁻¹, a threshold voltage of -0.54 V, and good PBTS reliability were obtained from the IGZO621:H TFTs with the 68 nm thick fluorinated Al₂O₃ GI. We found that fluorine in the AlOF_x formed at the Al₂O₃ surface played an important role in improving the performance and PBTS reliability of low-temperature-processed oxide TFTs for future flexible device applications.

ORCID iDs

Yusaku Magari  <https://orcid.org/0000-0001-9655-4283>
 S. G. Mehadi Aman  <https://orcid.org/0000-0003-2275-3751>
 Hiroshi Furuta  <https://orcid.org/0000-0002-3129-0894>
 Mamoru Furuta  <https://orcid.org/0000-0003-1685-3246>

- 1) M. Ito, M. Kon, M. Ishizaki, and S. Sekine, Proc. Int. Display Workshops in conjunction with Asia Display 2005 (IDW/AD'05), 2005, p. 845.
- 2) T. Hirao, M. Furuta, H. Furuta, T. Matsuda, T. Hiramatsu, H. Hokari, and M. Yoshida, SID Int. Symp. Dig. Tech. Papers, 2006, p. 18.
- 3) S. Park, C. Hwang, J. Lee, S. Chung, Y. Yang, L. Do, and H. Chu, SID Int. Symp. Dig. Tech. Papers, 2006, (San Francisco), p. 25.
- 4) H. Inoue et al., *IEEE J. Solid-State Circuits* **47**, 2258 (2012).
- 5) S. Yoon, S. Kim, M. Park, and D. Yun, *ECS Trans.* **75**, 227 (2016).
- 6) S. Aihara et al., *IEEE Trans. Electron Devices* **56**, 2570 (2009).
- 7) T. Sakai, H. Seo, T. Takagi, M. Kubota, H. Ohtake, and M. Furuta, Proc. Int. Electron Devices Meeting (IEDM2015), 2015, p. 779.
- 8) K. Koike, M. Hashimoto, K. Tsuji, Y. Seiwa, K. Ogata, S. Sasa, M. Inoue, and M. Yano, *Appl. Phys. Express* **2**, 087001 (2009).
- 9) K. Takechi, S. Iwamatsu, S. Konno, T. Yahagi, Y. Abe, M. Katoh, and H. Tanabe, *Jpn. J. Appl. Phys.* **54**, 078004 (2015).
- 10) M. Lorenz, A. Lajn, F. Frenzel, H. Wenckstern, M. Grundmann, P. Barquinha, R. Martins, and E. Fortunato, *Appl. Phys. Lett.* **97**, 243506 (2010).
- 11) D. H. Lee, K. Nomura, T. Kamiya, and H. Hosono, *ECS Solid State Lett.* **1**, Q8 (2012).
- 12) G. T. Dang, T. Kawaharamura, M. Furuta, and M. W. Allen, *IEEE Trans. Electron Devices* **62**, 3640 (2015).
- 13) G. T. Dang, T. Uchida, T. Kawaharamura, M. Furuta, A. Hyndman, R. Martinez, S. Fujita, R. Reeves, and M. W. Allen, *Appl. Phys. Express* **9**, 041101 (2016).
- 14) J. KaczMarski, J. Grochowski, E. Kamińska, A. Taube, M. Borysiewicz, K. Pagowska, W. Jung, and A. Piotrowska, *IEEE Electron Devices Lett* **36**, 469 (2015).
- 15) Y. Magari, S. G. M. Aman, D. Koretomo, K. Masuda, K. Shimpo, and M. Furuta, *Jpn. J. Appl. Phys.* **59**, SGGJ04 (2020).
- 16) K. Nomura, H. Ohta, A. Takagi, T. Kamiya, M. Hirano, and H. Hosono, *Nature* **432**, 488 (2004).
- 17) T. Kamiya, K. Nomura, and H. Hosono, *Sci. Technol. Adv. Mater.* **11**, 044305 (2010).
- 18) T. Hirao, M. Furuta, T. Hiramatsu, T. Matsuda, C. Li, H. Furuta, H. Hokari, M. Yoshida, H. Ishii, and M. Kakegawa, *IEEE Trans. Electron Devices* **55**, 3136 (2008).
- 19) Y. Hanyu, K. Abe, K. Domen, K. Nomura, H. Hiramatsu, H. Kumomi, and T. Kamiya, *J. Disp. Technol.* **10**, 979 (2014).
- 20) T. Kamiya and H. Hosono, *ECS Trans.* **54**, 103 (2013).
- 21) S. G. M. Aman, D. Koretomo, Y. Magari, and M. Furuta, *IEEE Trans. Electron Devices* **65**, 3257 (2018).
- 22) D. Koretomo, Y. Hashimoto, S. Hamada, M. Miyanaga, and M. Furuta, *Jpn. J. Appl. Phys.* **58**, 018003 (2018).
- 23) S. G. M. Aman, Y. Magari, K. Shimpo, Y. Hirota, H. Makino, D. Koretomo, and M. Furuta, *Appl. Phys. Express* **11**, 081101 (2018).
- 24) D. Koretomo, S. Hamada, M. Mori, Y. Magari, and M. Furuta, *Appl. Phys. Express* **13**, 076501 (2020).
- 25) C. Liang, T. Luo, M. Feng, H. Cheng, and D. Su, *Mater. Chem. Phys.* **43**, 166 (1996).
- 26) M. Ue, F. Mizutani, H. Takaha, S. Takeuchi, K. Sugiyama, T. Nishiwaki, and N. Sato, *Electrochim. Acta* **47**, 217 (2001).
- 27) L. Lan and J. Peng, *IEEE Trans. Electron Devices* **58**, 1452 (2011).
- 28) L. Lan, M. Zhao, N. Xiong, P. Xiao, W. Shi, M. Xu, and J. Peng, *IEEE Electron Devices Lett* **33**, 827 (2012).
- 29) W. Cai, S. Park, J. Zhang, J. Wilson, Y. Li, Q. Xin, L. Majewski, and A. Song, *IEEE Electron Devices Lett* **39**, 375 (2018).
- 30) S. Kono, Y. Magari, S. G. M. Aman, M. Mori, H. Furuta, N. Fruehauf, and M. Furuta, Ext. Abstr. Solid State Devices and Materials, 2020, p. 661.
- 31) A. Olziersky, P. Barquinha, A. Vilàl, L. Pereira, G. Gonçalves, E. Fortunato, R. Martins, and J. Morante, *J. Appl. Phys.* **108**, 064505 (2010).
- 32) Y. Magari, H. Makino, and M. Furuta, *ECS J. Solid State Sci. Technol.* **6**, Q101 (2017).
- 33) Y. Magari, S. G. M. Aman, D. Koretomo, K. Masuda, K. Shimpo, H. Makino, M. Kimura, and M. Furuta, *ACS Appl. Mater. Interfaces* **12**, 47739 (2020).
- 34) L. Zheng, X. Cheng, D. Cao, G. Wang, Z. Wang, D. Xu, C. Xia, L. Shen, Y. Yu, and D. Shen, *ACS Appl. Mater. Interfaces* **6**, 7014 (2014).
- 35) I. Iatsunskiy, M. Kempinski, M. Jancelewicz, K. Zalewski, S. Jurga, and V. Smyntyna, *Vacuum* **113**, 52 (2015).
- 36) R. Ramos, G. Cunge, B. Pelissier, and O. Joubert, *Plasma Sources Sci. Technol.* **16**, 711 (2007).
- 37) H. Yamazaki et al., *ECS J. Solid State Sci. Technol.* **3**, Q20 (2014).
- 38) J. Jiang, T. Toda, M. Hung, D. Wang, and M. Furuta, *Appl. Phys. Express* **7**, 114103 (2014).
- 39) M. Furuta, J. Jiang, M. Hung, T. Toda, D. Wang, and G. Tatsuoka, *ECS J. Solid State Sci. Technol.* **5**, Q88 (2016).
- 40) M. Miyakawa, M. Nakata, H. Tsuji, H. Iino, and Y. Fujisaki, *AIP Adv.* **10**, 065004 (2020).